POAC'25
St. John's, Newfoundland and Labrador, Canada

Proceedings of the 28th International Conference on Port and Ocean Engineering under Arctic Conditions
Jul 13-17, 2025
St. John's, Newfoundland and Labrador
Canada

A follow-up on the second set of Ice Impact Experiments with the Large Double Pendulum Apparatus

Sthefano L. Andrade[1], Robert E. Gagnon[2], Bruce W. Quinton[1]
[1] Memorial University of Newfoundland, St. John's, Canada
[2] National Research Council Canada, St. John's, Canada

ABSTRACT

This article reports on the experimental parameters, ice specimen characteristics, force data, pressure data, and ice specimen penetration data for five ice impact experiments on a rigid panel. Three impacts were performed three with ice cones and two with approximately spherical ice caps. This series of experiments resulted in the highest ice load measured with the Large Pendulum Apparatus, peaking at 1.025 MN. As initially reported by Gagnon et al., 2024, the pressure plugs have been confirmed capable of resolving spallation events. Additionally, some of these events were captured on video by the high-speed cameras, and these events also induced sudden changes in the force magnitude and distribution as measured by the load cells.

KEYWORDS: Ice impacts; Pressure sensing; Double-pendulum apparatus; Impact panel.

INTRODUCTION

This paper is the second paper on the ice impact experiment series performed as collaboration between MUN (Memorial University of Newfoundland) and NRC (National Research Council Canada). In these experiments ice specimens of conical and spherical cap shapes impacted a rigid panel instrumented with pressure sensors. The first paper is titled "Large Double-Pendulum Ice Impact Tests – Phase II" by Gagnon et al. (2024) and it discusses the results and findings for the first impact of the series and general setup. The current paper presents the results for the remaining ice impacts.

The large double pendulum apparatus was first presented in (Gagnon et al., 2015). The first series of impacts measured ice pressure distribution observed in ice cone impacts against a rigid pressure sensing apparatus (Gagnon et al., 2020; Sopper et al., 2015). A second series of experiments was then conducted with deformable panels and an upgraded pendulum (Lande Andrade et al., 2023). The results include measured loads, post-impact panel permanent

deformation, and pendulum displacements / velocities determined through the analysis of high-speed videos using digital image correlation (DIC), however no localized pressures were measured.

Recently a rigid panel with a pressure sensing array was designed to be installed in the Pendulum to measure local pressure of ice and the first impact results were reported and discussed in Gagnon et al. (2024). The type of pressure-sensor array used in the current experiments has been used in the past (e.g., Masterson et al., (1993)) for low-speed ice indentation experiments, and for higher-speed impact tests (e.g., Timco and Frederking, (1993); Chin and Williams, (1989); Gagnon and Gammon, (1997)).

EXPERIMENTAL SETUP

The large pendulum setup was previously presented in detail (Gagnon et al., 2024; Lande Andrade et al., 2023). Figure 1 shows that it consists of two pendulums, the left carriage holds the ice indenter, and the right carriage holds the impacted panel, in this case a rigid panel instrumented with the pressure-sensor array.

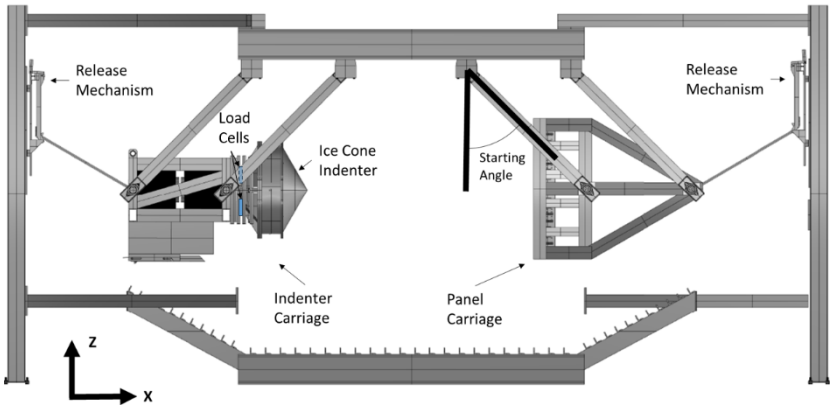

Figure 1. Double Pendulum Main Components. Side View. (adapted from Lande Andrade et al., (2023)).

The ice specimen carriage is equipped with three force measuring load cells (Kistler 9091B, 1200 kN, piezoelectric load cells). The panel is equipped with a pressure-sensor array, illustrated in Figure 2. The panel is stiffened vertically and horizontally, and it was designed to have small elastic deformation for the tested loads. The sensor labelled as #1 is located at the first point of contact between ice specimen and the rigid panel during the impact. The pressure plug contact area is 124.7 mm^2. In Figure 2 The reader will note that the impact region of the panel (the light-colored square) has been machined to be smooth and uniformly flat, where the aim was to reduce the influence of local geometric imperfections on the ice fracture mechanisms.

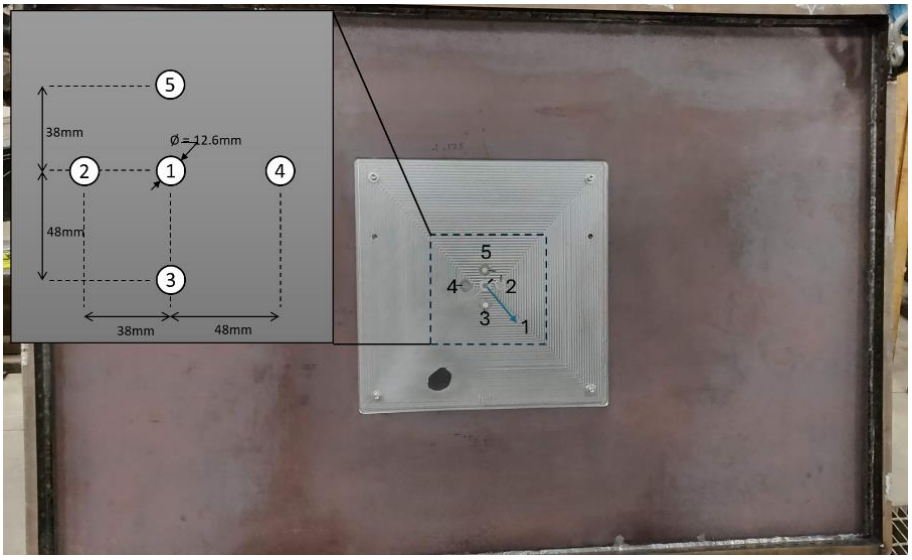

Figure 2. The rigid panel and the pressure sensing array.

Ice Test Specimens

The spherical cap and cone-shaped ice test specimens are shaped from an ice cylinder core, as illustrated in Figure 3. The ice cylinder growing process has been carefully described in previous works (Gagnon et al., 2024, 2020; Gudimetla et al., 2012). In brief, the ice cylinders are grown from filtered freshwater, they have granular structure achieved by seeding it with roughly 11 mm diameter ice grains. The chilled water is poured into the container filled with ice grains, while stirring the mixture during filling to release trapped air. The ice/water mixture freezes from the bottom up, to avoid stress concentrations. The room temperature during freezing was between -15 and -25 $^{\circ}$C.

The ice cone shaping is straight-forward. The ice cylinder has a diameter of 1m. The specimen is placed on a turntable and the blade is lowered until the specimen has a vertex opening angle of 120°. Conversely, the spherical samples are shaped by hand with suitable power tools, following a reference shape made of Styrofoam. This introduces some variability in their dimensions, as illustrated in Figure 4. More information on geometry is available in Figure 5 and Table 1.

Figure 3. Ice cylinder before shaping (left). Ice cone being shaped (centre). Hemispherical ice cap being shaped by hand (right).

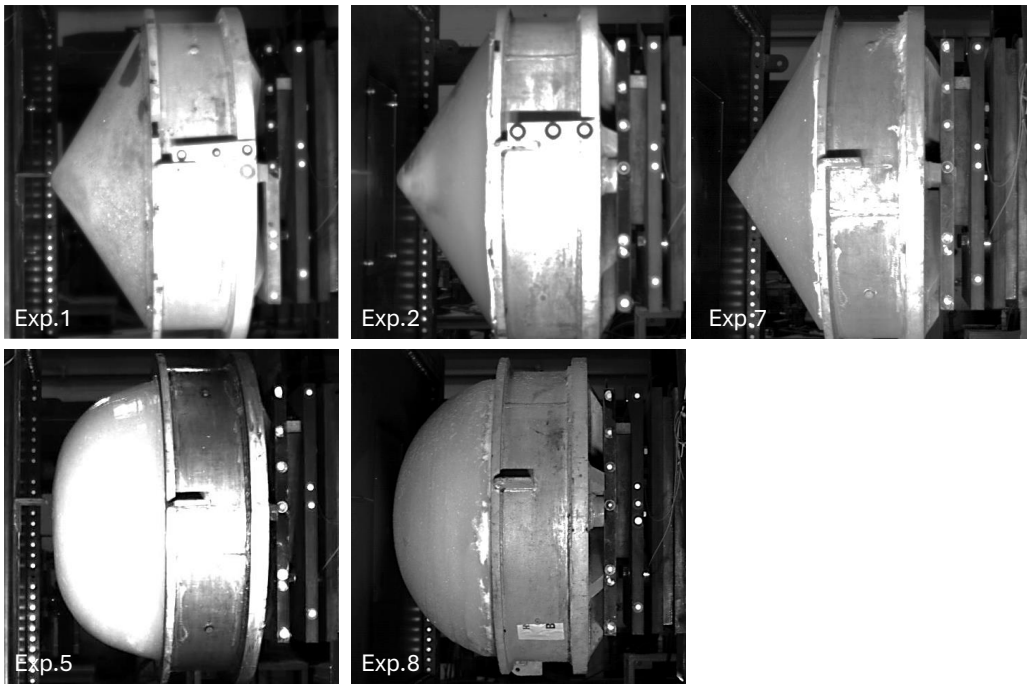

Figure 4. Ice specimen profiles for all experiments conducted. Nomenclature is based on the test program designation.

Table 1 briefly summarizes the variations for each ice specimen. Impacts 3 and 4 are a separate project.

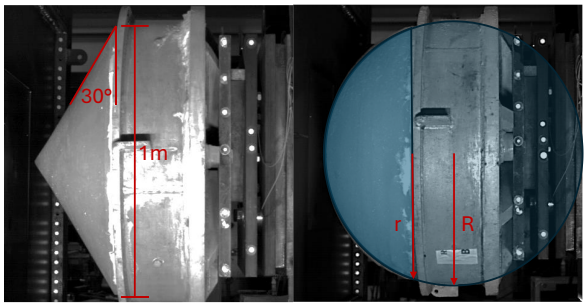

Figure 5. Typical geometry of the specimens. Cone on the left, spherical cap on the right.

Table 1. Summary of the ice specimens'.

Experiment	**Specimen Type / Dimensions / (Core temperature)**	**Notes**
Impact 1	Cone. (-6 °C)	Typical Cone
Impact 2	Cone. (-5 °C to -9 °C)	Due to a power outage the top of the cylinder melted and re-froze during storage.
Impact 5	Spherical Cap. (-1 °C to -1.4 °C) r: 0.493 m R :0.580 m	High ice temperature. Specimen's shape accuracy is not ideal (excessively flat top surface).
Impact 7	Cone (-15 °C)	Typical Cone
Impact 8	Spherical Cap (-15 °C) r: 0.5 m R: 0.523 m	Typical spherical cap

* Temperature sampled at the ice core post impact.

RESULTS

This section presents the data from the five impact experiments. Force, and penetration data are included here. Note that force data is sampled at 100 kHz with a LPF (low-pass filter) of 2 kHz. Pressure is sampled at 100 kHz with a LPF of 10 kHz. And the high-speed cameras record at 1 kHz.

The time origin of all force plots is defined as the instant when the total force of all load cells first rises. Ice penetration is determined with DIC analysis, and the time origin is defined as the first image frame before contact between the ice and the rigid panel. Table 2 summarizes the equivalent mass of the ice specimen carriage (IC) and panel carriage (PC), the relative impact speeds, and kinetic energy for all experiments.

Table 2. Experimental impact parameters.

Experiment	Equivalent Mass* IC / PC [kg]	Drop Angle IC / PC [degree]	Relative Impact Speed Theoretical / DIC determined [m/s]	Kinetic Energy Theoretical / DIC determined [kJ]
1	4723 / 4759	50.85 / 50.15	7.56 / 7.47	67.7 / 66.1
2	4723 / 4759	50.85 / 50.15	7.56 / 7.53	67.7 / 67.2
5	4813 / 4759	40.65 / 40.40	6.14 / 6.10	45.0 / 44.5
7	4723 / 4759	49.85 / 50.10	7.48 / 7.52	66.4 / 66.9
8	4813/ 4759	40.40 / 40.40	6.12 / 6.00	44.8 / 43.1

* The equivalent mass includes the effective mass of the pendulum arms.

Below, we have organized the results of the impacts into 2 groups: ice cone impacts and spherical ice cap impacts. The collisions can be assumed inelastic (negligible rebound).

Ice Cone Impacts

The ice cone impact force, impulse, and penetration data are presented in this section. Figure 6 presents the force data and Figure 7 the impulse load calculation plot, which was calculated by integrating the force-time curves for the duration of the impact.

Table 3 summarizes force data, impact duration, impulse for Impacts 1, 2, and 7. For comparison, Gagnon et al. (2020) reports that, for drop angles of 35° -with impact energies approaching 29 kJ (Andrade et al., 2020) -peak loads varied from 416 kN at 0.015 s to 622 kN at 0.017 s, and impact durations varied from 0.048 s to 0.079 s. The results of another experiment (Lande Andrade et al., 2023), with a fresh ice cone impact performed against a deformable panel, reported a peak impact force of 553 kN, impact duration of 0.055 s, and average force of 282 kN.

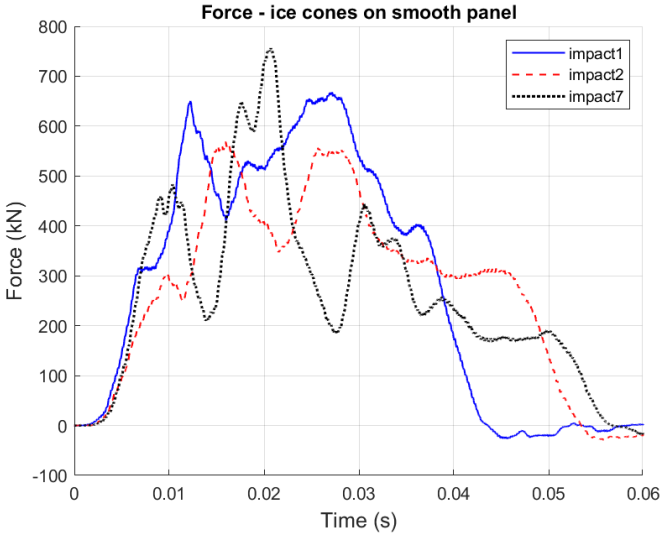

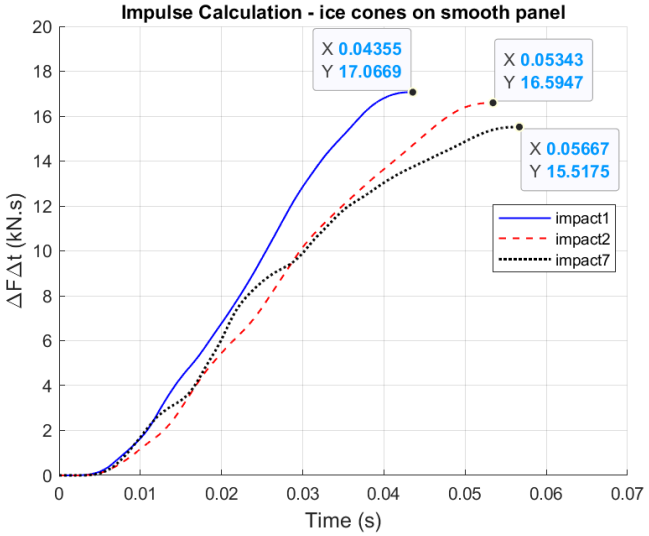

Figure 6. Ice cones force data for the impact duration. Figure 7. Calculated impulse load of the ice cones.

Table 3. Peak force and impulse information for ice cone impacts.

Impact #	Peak Force [kN]	Peak Load time [s]	Average Force [kN]	Total Duration [s]	Impulse [kN.s]
1	667.8	0.0272	391.5	0.0436	17.1
2	569.3	0.0159	310.5	0.0534	16.6
7	756.2	0.0207	273.8	0.0567	15.5

The ice penetration over time is determined by DIC and it is the relative displacement between the right and left carriages in Figure 1, where it is reasonable to consider the stiff impact panel as rigid. Figure 8 presents the measured indentations of the ice cone specimens using the DIC data. The values are presented up to the point where ice penetration ceases.

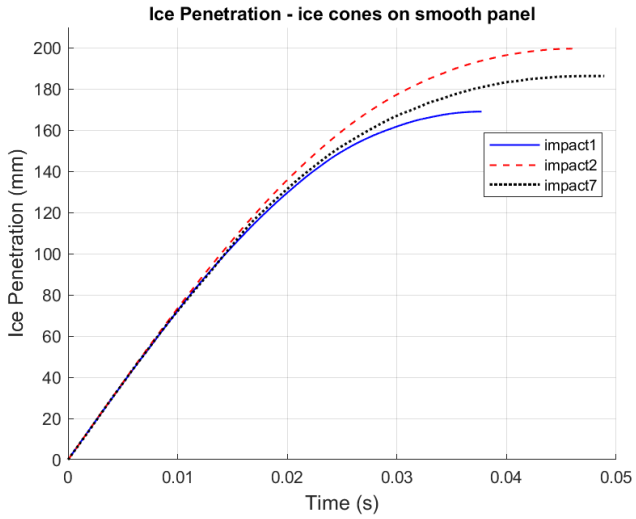

Figure 8. Penetration curves for the ice cones.

Spherical ice cap impacts

The spherical ice caps impact force, impulse, and penetration data are presented in this section. Figure 9 presents the force data and Figure 10 the impulse data. Table 4 presents the maximum values for force and impulse, average force and impact duration.

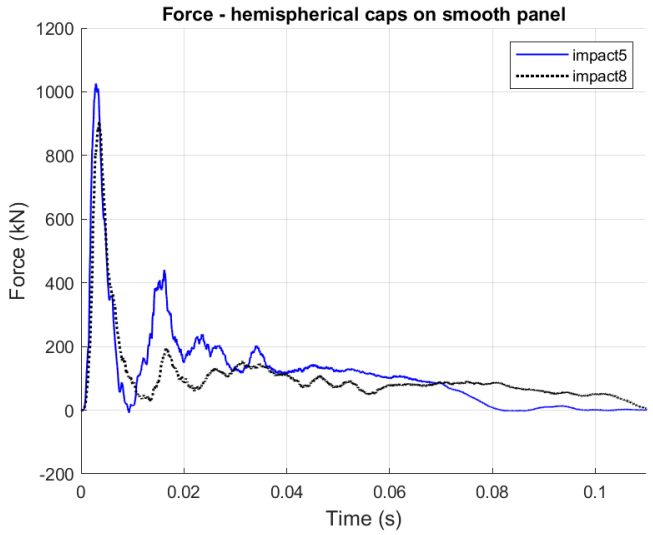

Figure 9. Spherical ice caps force data for the impact duration.

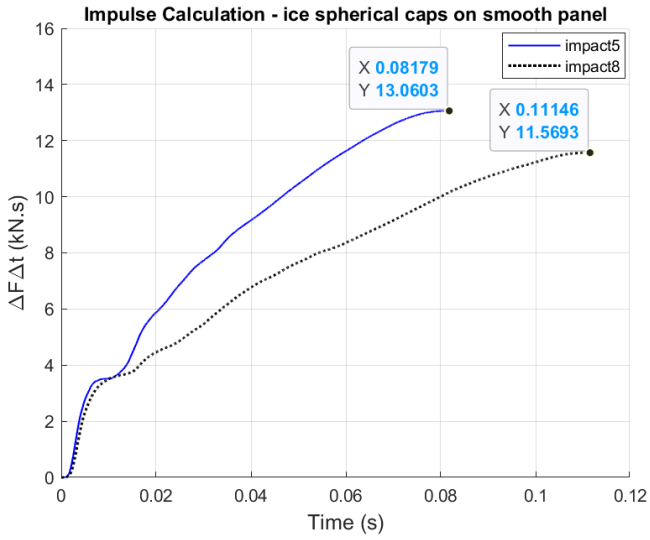

Figure 10. Calculated impulse of the spherical ice caps.

Table 4. Peak force and impulse information for spherical ice cap impacts.

Impact #	Peak Force [kN]	Peak Load time [s]	Average Force [kN]	Total Duration [s]	Impulse [kN.s]
5	1026	0.0029	160	0.0818	13.1
8	906	0.0035	104	0.1115	11.6

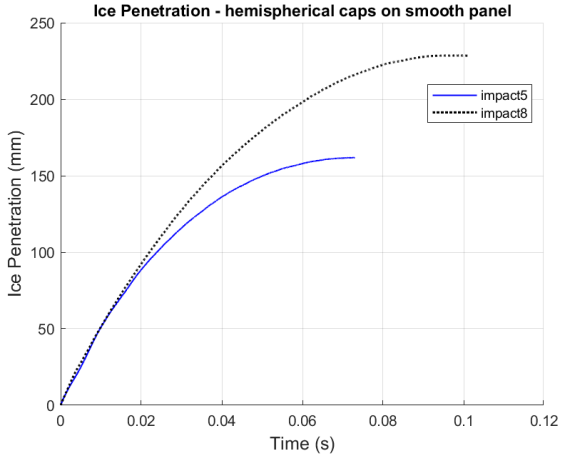

Figure 11. Penetration curves of the spherical ice caps.

Summary of pressure data

Table 5 shows that the pressure data collected is consistently higher for the ice-cone impacts than the spherical ice caps.

We also note, as indicated in Figure 12, evidence of spallation events early in the impact 7-pressure record from a cone-shaped ice impact, which is similar to data reported earlier by Gagnon et al. (2024) using the same impact apparatus and similar ice specimens.

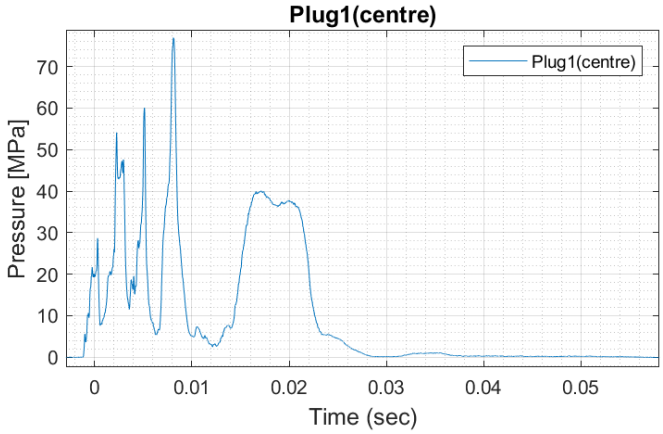

Figure 12. Impact 7 pressure plug 1 data.

Table 5. Average and maximum pressure for each impact test.

Experiment	1	2	5	6	7	8
Average Pressure	7.0 MPa	4.9 MPa	2.0 MPa	4.8 MPa	7.0 MPa	2.4 MPa
Max. Pressure	33.1 MPa	34.7 MPa	25.7 MPa	28.8 MPa	76.9 MPa	37.1 MPa

DISCUSSION

When compared to ice cone impacts, spherically shaped ice specimens show a much higher peak force for impacts with approximately 67% of the kinetic energy. Impact 5 and 8 have high peak loads, but their average loads are significantly lower than the ice cone impacts, and the impact durations are much longer, even though the spherical cap crushable volume, using nominal contact areas, is 2.2x larger than that of the cones. This illustrates the importance of shape on the ice behaviour and load application (examples of other works that discuss this topic include, but are not limited to, Frederking et al., 1990; Bruneau et al., 2013; Habib et al., 2014; Birajdar et al., 2016; Müller et al., 2024).

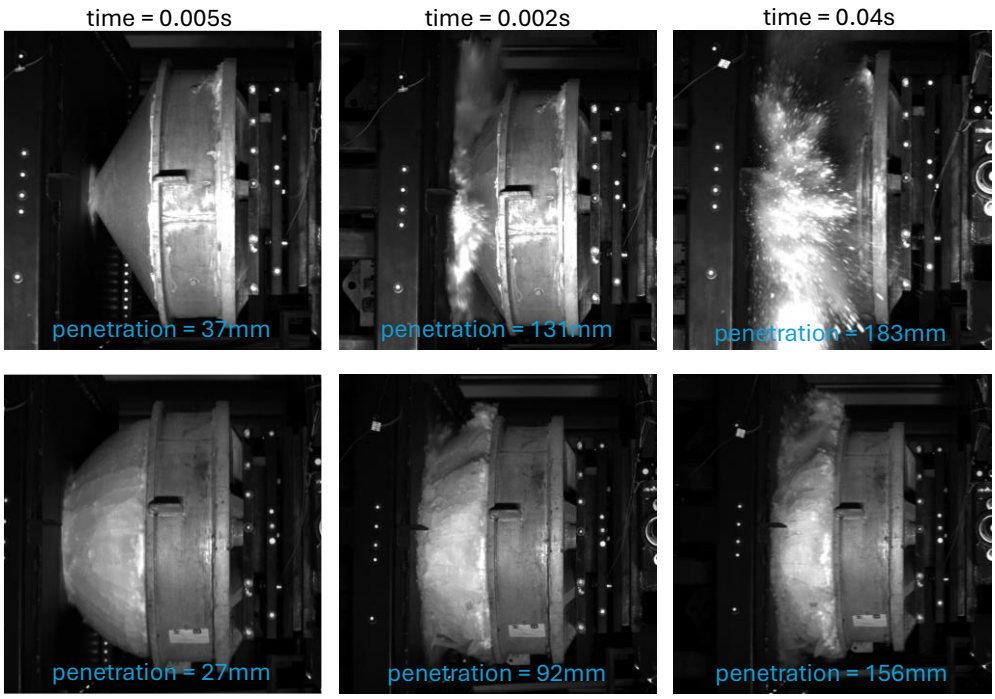

Figure 13. Behaviour comparison between cones and spherical cap ice specimens.

Another interesting behaviour can be seen in Figure 13. It shows that the cone is maintaining its shape during collision while the spherical cap is fracturing catastrophically at lower penetration levels. This is related to the dramatically different ice-contact-area versus penetration profiles (and load profiles) that the two ice shapes have in the early stages of the impacts, such as at time 0.005 s (left images in Figure 13). The difference between spherical and cone-shaped ice specimen behaviour observed in these experiments is related to the spallation aspects. As observed and discussed by other authors spallation is an important phenomenon in ice compressive failure during high strain-rate indentation (e.g., Taylor and Jordaan, 2015; Andrade et al., 2023). In the current study, it was observed that spherical ice indenters exhibit larger spallation events early in the impact process, as opposed to the ice cone tests where large spallations occurred later in the impact. Shape confinement is much more effective in the low-profile cone-shaped ice than in the higher-profile roughly hemispherical-shaped ice samples.

This behaviour also explains the longer duration and higher penetration of impacts with spherical caps (Figure 11), since only a relatively small amount of the available kinetic energy is dissipated during the initial high load peak that occurs with the spherical-cap specimens. The remaining kinetic energy must then be dissipated by relatively easy penetration into highly damaged ice, leading to lower load and longer penetration than that of the cone-shaped specimens.

The effects of confinement in cones and its relation with tapering angle also have been discussed in the works of Bruneau et al., 2013 and Habib et al., 2014. The authors show that tapering angle (i.e., bulk shape confinement) play an important rule in the way the specimen behaves during high strain-rate events, with lower tapering angles usually leading to larger and

more prominent spallation events, but delivering more energy per crushed volume. The authors also discuss the effect of strain-rate and temperature on ice compressive behaviour. In this work, all tests performed place ice failure well within the brittle regime, and show some mix of crushing and large spallations, similar to what was observed in other works. As for the influence of temperature, the sample size presented here is not large enough to draw any significant comparison. On a final note, the ice shapes studied in Muller et al were based on shaped ice cylinders, so the base of the shape was not confined in any way. This limits comparison between the presented work and their work.

CONCLUSIONS

This work presents the force, impulse, and penetration data for five ice impact experiments against a rigid panel instrumented with pressure sensors. Two shapes of ice specimens were used in the tests, conical and spherical cap. The conical specimens had roughly 67 kJ of kinetic energy at the instant of the impact, while spherical cap specimens had approximately 44 kJ. The spherical specimens generated the highest peak loads, 906 kN and 1026 kN, with impact durations of 0.11 s and 0.0818 s, impulses of 11.6 kN.s and 13.1 kN.s, but with lower average forces, 104 kN and 160 kN, when compared to ice cone impacts. The ice cone impacts had peak loads ranging from 569 kN to 756 kN, duration of 0.044 s to 0.057 s, impulses between 15.5 kN.s and 17.1 kN.s, and average forces of 274 kN to 391 kN. The high-speed camera data shows that spherical caps are prone to catastrophic fracture of the entire specimen early in the impact process, while ice cones retain their shape much better, thus being able to sustain load more consistently throughout the impact event. This observation corroborates with the pressure data that show consistently higher values for the ice-cone impacts than the spherical ice cap impacts.

Future work will include the in-depth analysis of measured pressure distribution and its relation to the different tested shapes. Additionally, a thorough energy dissipation analysis will be included in such work, including energy per crushed volume.

AKNOWLEDGEMENT

The authors are grateful to Memorial University and the National Research Council for supporting this work under their joint-research KARLUK Program.

REFERENCES

Andrade, S.L., Gagnon, R., Colbourne, B., Quinton, B.W., 2023. Ice pressure distribution model: A geometry-based solution for high-pressure zone representation. Cold Regions Science and Technology 210, 103822–103822. https://doi.org/10.1016/j.coldregions.2023.103822

Andrade, S.L., Quinton, B.W.T., Daley, C.G., Gagnon, R.E., 2020. Numerical Study of Large Pendulum Ice Impact Loads. Presented at the Volume 7: Polar and Arctic Sciences and Technology, American Society of Mechanical Engineers, Virtual, Online, pp. 1–10. https://doi.org/10.1115/OMAE2020-19068

Birajdar, P., Taylor, R., Habib, K., Hossain, R., 2016. Analysis of Medium-Scale Laboratory Tests on Ice Crushing Dynamics, in: All Days. Presented at the Arctic Technology

Conference, OTC, St. John's, Newfoundland and Labrador, Canada, p. OTC-27482-MS. https://doi.org/10.4043/27482-MS

Bruneau, S., Colbourne, B., Dragt, R., Dillenburg, A., Ritter, S., Pilling, M., Sullivan, A., 2013. LABORATORY INDENTATION TESTS SIMULATING ICESTRUCTURE INTERACTIONS USING CONE-SHAPED ICE SAMPLES AND STEEL PLATES, in: Proceedings of the 22nd International Conference on Port and Ocean Engineering under Arctic Conditions. Presented at the POAC, Espoo, Finland.

Chin, S.N., Williams, F.M., 1989. Measurement of impact forces on sea ice, in: 10th International Conference on Port and Ocean Engineering under Arctic Conditions, 12-16 June 1989, Luleå, Sweden. Collection / Collection : NRC Publications Archive / Archives des publications du CNRC.

Frederking, R.M.W., Jordaan, I.J., McCallum, J.S., 1990. Field Tests of Ice Indentation at Medium Scale Hobson's Choice Ice Island, 1989. Presented at the IAHR, Espoo, Finland, pp. 931–944.

Gagnon, R., Andrade, S.L., Quinton, B.W., Daley, C., Colbourne, B., 2020. Pressure distribution data from large double-pendulum ice impact tests. Cold Regions Science and Technology 175, 103033–103033. https://doi.org/10.1016/j.coldregions.2020.103033

Gagnon, R., Daley, C.G., Colbourne, B., 2015. A large double-pendulum device to study load, pressure distribution and structure damage during ice impact tests in the lab. Presented at the Proceedings of the 23rd International Conference on Port and Ocean Engineering under Arctic Conditions, POAC, Trondheim, Norway, pp. 1–10.

Gagnon, R., Quinton, B., Lande Andrade, S., 2024. Large double-pendulum ice impact tests – phase II. https://doi.org/10.5281/ZENODO.14531592

Gagnon, R.E., Gammon, P.H., 1997. In situ thermal profiles and laboratory impact experiments on iceberg ice. Journal of Glaciology 43, 569–582. https://doi.org/10.1017/S0022143000035188

Gudimetla, P.S.R., Colbourne, B.D., Daley, C.G., Bruneau, S.E., Gagnon, R., 2012. Strength and pressure profiles from conical ice crushing experiments. Presented at the International Conference and Exhibition on Performance of Ships and Structures in Ice 2012, ICETECH 2012, Banff, Canada, pp. 167–174.

Habib, K.B., Taylor, R.S., Jordaan, I.J., Bruneau, S., 2014. Experimental Investigation of Compressive Failure of Truncated Conical Ice Specimens, in: Volume 10: Polar and Arctic Science and Technology. Presented at the ASME 2014 33rd International Conference on Ocean, Offshore and Arctic Engineering, American Society of Mechanical Engineers, San Francisco, California, USA, p. V010T07A044. https://doi.org/10.1115/OMAE2014-24184

Lande Andrade, S., Elruby, A.Y., Hipditch, E., Daley, C.G., Quinton, B.W.T., 2023. Full-scale ship-structure ice impact laboratory experiments: experimental apparatus and initial results. Ships and Offshore Structures 18, 500–514. https://doi.org/10.1080/17445302.2022.2032993

Masterson, D.M., Frederking, R.M.W., Jordaan, I.J., Spencer, P. A., 1993. Description of multi-year ice indentation tests at Hobson's Choice Ice Island—1990, in: Proceedings of the 12th International Conference on Offshore Mechanics and Arctic Engineering. Presented at the OMAE, Glasgow, United Kingdom.

Müller, F., Böhm, A., Herrnring, H., Von Bock Und Polach, F., Ehlers, S., 2024. Influence of the ice shape on ice-structure impact loads. Cold Regions Science and Technology 221, 104175. https://doi.org/10.1016/j.coldregions.2024.104175

Sopper, R., Gagnon, R., Daley, C., Colbourne, B., 2015. Measurements of spatial and temporal

variations in ice impact pressures. Presented at the Proceedings of the International Conference on Port and Ocean Engineering under Arctic Conditions, POAC, Trondheim, Norway.

Taylor, R.S., Jordaan, I.J., 2015. Probabilistic fracture mechanics analysis of spalling during edge indentation in ice. Engineering Fracture Mechanics 134, 242–266. https://doi.org/10.1016/j.engfracmech.2014.10.021

Timco, G.W., Frederking, R.M.W., 1993. Laboratory impact tests on freshwater ice. Cold Regions Science and Technology 22, 77–97. https://doi.org/10.1016/0165-232X(93)90047-C